On the Breakup of Fluid Particles in Turbulent Flows

Ronnie Andersson and Bengt Andersson
Dept. of Chemical and Biological Engineering, Chalmers University of Technology, SE-41296, Gothenburg, Sweden

DOI 10.1002/aic.10831
Published online March 24, 2006 in Wiley InterScience (www.interscience.wiley.com).

Dynamics of bubble and drop breakup in turbulent flows have been studied in detail, using a high-speed CCD camera. Analysis of breakup times, deformations, deformation velocities, number of fragments, and the resulting daughter size distributions show that there are several important differences in the breakup mechanism of bubbles and drops. It is shown that the increase in interfacial energy prior to breakup exceeds the increase after breakup. The use of an activation barrier that better describes the turbulent structures that can interact with fluid particles and also cause breakup is proposed. Measurements under identical hydrodynamic conditions reveal that an internal flow redistribution mechanism is responsible for generation of unequal-sized bubble fragments. Due to the three orders of magnitude higher density of liquids than of gases, this mechanism does not occur for drops. The measurements also show that assumption of binary breakup is reasonable for bubbles but not for drops. © 2006 American Institute of Chemical Engineers *AIChE J,* 52: 2020–2030, 2006
Keywords: breakup, deformation, drop, bubble, fluid particle, daughter size distribution, turbulence, binary and multiple breakup, high-speed imaging technique

Introduction

Breakup of fluid particles in turbulent flows is one of the most important processes in reaction engineering. Hence, accurate predictions of breakup rates become important not only in the chemical industries but also in the pharmaceutical, food, and petroleum industries. Unfortunately, the breakup rate models proposed in the literature give contradictory predictions.[1] Many of the models are derived from assumptions that have not been validated experimentally. Others contain adjustable parameters, which make them less useful. To advance the development of theoretical breakup rate models, it is necessary to experimentally investigate the breakup mechanism in detail. The breakup process occurs on very small scales, so the measurements must be done with high enough spatial and temporal resolution. In this article such a technique is devised and the breakup mechanisms of fluid particles are studied in detail. Traditionally, no distinction between the breakup mechanism of bubbles and drops has been made in the model development. As shown in this article, there are several differences between bubble and drop breakup that must be accounted for.

Correspondence concerning this article should be addressed to B. Andersson at bengt.andersson@chalmbers.se.

Breakup of Fluid Particles—Literature Review

Breakup of fluid particles in turbulent flows has been a subject of investigation for many years, starting with the pioneering work of two researchers, Kolmogorov[2] and Hinze,[3] and generated numerous publications in the intervening decades. The early work mainly focused on determining correlations for the maximum stable fluid particle diameters, d_{max}, and the average fluid particle diameter, d_{32}, under various operating conditions.

Recent work has mainly focused on deriving theoretical breakup rate models that contain no adjustable model parameters. These models have been used with various degrees of success in CFD-population balance simulations.[4,5] Validation of the models has been done mainly by measurements of the

average diameters and the evolution of the size distributions. No distinction has yet been made between the breakup mechanism of drops and bubbles. The fact that no unifying breakup model has been found implies that the phenomenon is not well understood.

Breakup stresses

Stress analysis can be used to determine whether breakup occurs or not. A fluid particle immersed in a turbulent flow experiences turbulent stresses, that is, viscous stress and dynamic pressure, that act to deform and disrupt the particle. Breakup occurs when the fluid particles are exposed to disruptive stresses that exceed the cohesive stresses. Both turbulent shear stress and turbulent normal stress may cause breakup. Thus, contrary to laminar flow, breakup of fluid particles can occur regardless of the dispersed phase viscosity.[6] The cohesive forces counteract the disruptive forces and tend to restore the fluid particle to spherical form. The main cohesive stress is the interfacial tension. Small fluid particles and particles with high enough viscosity are also stabilized due to the internal stress.

By comparing the disruptive and cohesive stresses, a criterion can be specified for the occurrence of breakage. Assuming that there is no difference in the mean velocities of the two phases, the disruptive stress is given by the dynamic pressure fluctuations caused by turbulent structures within a given interval. Turbulent structures larger than the fluid particles are commonly assumed to only cause translation displacement. Hence, only turbulent structures of a size equal to or less than the fluid particles are assumed to cause breakup. To determine the magnitude of the dynamic pressure fluctuations of these turbulent structures, it is assumed that they fall within the inertial sub-range. The disruptive dynamic pressure fluctuations of a turbulent structure of a given size is then:

$$\tau \propto \rho_c \overline{u_\lambda^2}/2 \tag{1}$$

where $\overline{u_\lambda^2}$ is the mean squared velocity difference over the distance, λ. In the inertial sub-range the velocity fluctuation is given by

$$\overline{u_\lambda^2} = c_1(\varepsilon\lambda)^{2/3} \simeq 2.0(\varepsilon\lambda)^{2/3}. \tag{2}$$

In contrast to single phase flow for which continuous processes such as mixing can be described well with the average energy, the breakup of fluid particles is a discrete process. This means that if the energy is not quite sufficient to cause breakup, the fluid particle would only stretch before it relaxes to its original spherical shape. The relaxation process is followed by a few cycles of oscillation with decreasing amplitude, during which the interfacial energy that was supplied by the turbulent structure is dissipated. Hence, in contrast to continuous processes for which an average can be used, the energy distribution around the mean becomes more critical in describing the outcome of a discrete process such as breakup. Knowledge about this kind of energy distribution is limited. It is often assumed that the energy distribution is given by[7]:

$$P(e(\lambda)) = \frac{1}{\bar{e}(\lambda)} \exp(-e(\lambda)/\bar{e}(\lambda)) \tag{3}$$

where $\bar{e}(\lambda)$ is the mean turbulent kinetic energy of the eddy,

$$\bar{e}(\lambda) = \rho_c \frac{\pi\lambda^3}{6} \frac{\overline{u_\lambda^2}}{2}. \tag{4}$$

Thus, the energy distribution around the mean energy is independent of the size of the turbulent structure. This probability distribution of energies and resulting distribution of the disruptive stresses appears in many breakup models.

Among the stresses counteracting the disruptive stresses, the interfacial stress is generally the most important. This stress is given by:

$$\tau \propto \frac{\sigma}{d}. \tag{5}$$

Here, σ is the interfacial tension and d is the diameter of the fluid particle. In addition, the internal viscous stress may also contribute to the stabilization of the fluid particles. The internal viscous stress is given by:

$$\tau \propto \frac{\mu_d}{d} \sqrt{\frac{\tau_{ext}}{\rho_d}}. \tag{6}$$

Equation 6 shows that the internal viscous stress is proportional to the internal viscosity and inversely proportional to the size of the fluid particle. Hence, this stress is negligible for large gas bubbles, whereas it can significantly contribute to the stabilization of small viscous liquid drops. The Ohnesorge number $Oh = \mu_d/(\rho_d d\sigma)^{1/2}$ describes the relative importance of the two stabilizing stresses. Hinze[3] proposed that the breakup occurs when the disruptive stresses exceed the cohesive stresses:

$$\tau d > \sigma + \mu_d \sqrt{\tau_{ext}/\rho_d}. \tag{7}$$

The maximum stable diameter exists when the disruptive stress balances the cohesive stress. Disregarding internal viscous stress, Eq. 8 gives the maximum stable diameter of a fluid particle immersed into a turbulent field:

$$d_{\max} \propto \left(\frac{\sigma}{\rho_c}\right)^{0.6} \varepsilon^{-0.4}. \tag{8}$$

Experimental studies on the maximum stable diameter, carried out during a long time, have shown that the second exponent in Eq. 8 changes with time. In fact, a drift in the maximum stable diameter has been observed even after several hours in an STR. This is believed to be an effect of turbulence intermittency.[8] In light of Eq. 3, it is easily understood that time plays an important role in the breakup of fluid particles. The probability distribution of energies implies that experimental studies of single breakup events must account for either long

enough residence time or a large enough number of observations of breakup events so that the fluid particles have been subjected to the largest disruptive stress. However, in most studies, this criterion has not been fully considered, which can explain some of the disagreement in observations of the maximum stable diameters reported in the literature.[9] Although the stress analysis explains under what conditions a fluid particle breaks up, it does not predict at what rate breakup occurs.

Experimental observations on bubble and drop breakup

Sleicher studied the breakup of drops in turbulent flows and found that binary breakup results in a distribution of daughter drop sizes.[10] He found that most breakups generated equal-sized fragments. Collins and Knudsen, who photographed drop dispersions, observed that highly deformed drops existed in the flow.[11] The still photographs showed that the deformed drops had a dumbbell shape, with two spherical ends connected by a long cylinder. Konno et al., who studied the breakup of drops in turbulent flows, concluded that multiple fragmentation occurs.[12]

Walter and Blanch studied bubble breakup and identified three stages that characterize the breakup mechanism: oscillation, dumbbell stretching, and pinching off.[13] It was concluded from the study that two fragments were formed. No information about the final size distributions was given.

Hesketh et al., who studied both drop and bubble breakup, reported that only binary breakup occurred in the turbulent pipe flow they studied.[14] They observed that unequal-sized breakup was much more probable than equal-sized breakup both for bubble and drop breakup.

Risso and Fabre studied the breakup of bubbles under microgravity conditions aboard an aircraft flying in parabolic trajectories to avoid any possible buoyancy driven breakup mechanism besides the turbulent breakup.[9] They concluded that two mechanisms were responsible for breakup: the first was a resonance one and the second was an eddy-bubble deformation breakup mechanism that occurs without previous oscillations. The authors concluded that the second mechanism was more frequently encountered under their experimental conditions. They also concluded that only eddies close in size to the bubble diameter determine the breakup. Most of the breakup was binary, but breakup events resulting in up to 10 fragments were observed in the measurements.

Martinez-Bazan et al. studied primarily the evolution of the bubble size distribution in a turbulent liquid jet. However, they reported that breakage is mainly binary.[15] They observed multiple fragmentations at high turbulent Weber numbers, but gave no explanation. They conclude that the binary assumption holds for low to moderate Weber numbers, but that this assumption must be revised as the ratio of the disruptive to the cohesive forces increases.

Eastwood and colleagues measured drop breakup in a turbulent liquid jet.[16] They found that drops were considerably elongated before breakup. The deformation or stretching increased with rising drop viscosity. The stretching occurred on scales comparable to the turbulent integral length scale, and some deformed drops seemed to rotate with the turbulent structures. Although it was difficult for them to identify the number of fragments formed, they observed that multiple breakup occurred. No results on the daughter fragment sizes were given. They concluded that the results contradict the classical assumption that breakup is a result of interaction with turbulent velocity fluctuations over distances comparable to or smaller than the liquid drops. It was commented that there are similarities with breakup of drops in laminar flows. Another conclusion, drawn from comparison of the results from Eastwood et al. with those of Martinez-Bazan et al., is that bubble breakup scales with the classical Kolmogorov-Hinze theory for turbulent particle breakup, although the drop breakup does not. Instead, the Eastwood group found that the drop breakup scaled better with the large eddies in the background flow.

Two conclusions can be drawn by analyzing the results presented in the literature. The first conclusion is that the results often contradict each other. This is due to the fact that the experiments were performed in different equipments under different operating conditions for different fluids. This makes direct comparison of the results very difficult, if not impossible. The second conclusion is that the observations mainly concern the outcome from the breakup event, not the dynamics of the deformation and breakup process itself. Hence, a lot of information and details about the mechanism is lost. While the first studies were made with still image cameras, the development of high-speed digital cameras allows the mechanism to be studied in detail.

The objective of this article is to improve the understanding of the breakup process for fluid particles. Hence, experimental data on the breakup of both bubbles and drops in the same equipment under identical hydrodynamic conditions are needed. Detailed understanding of the phenomena also requires analysis of the deformation and breakup dynamics, not only the outcome from each breakup event.

Experimental Facility and Image Acquisition

A high-speed CCD camera allowing record rates up to 4000 Hz with a 10 bit dynamic resolution was used to record the rapid breakup processes. Short exposure times, typically on the order of 10-100 μs, were required to obtain sharp images of the fluid particles. A hybrid light measurement was used since it gave better images of deformed structures than the shadowgraph and the front light techniques. The hybrid light technique consists of a reflector and light sources located on the same side of the reactor as the camera, as shown in Figure 1. An intense

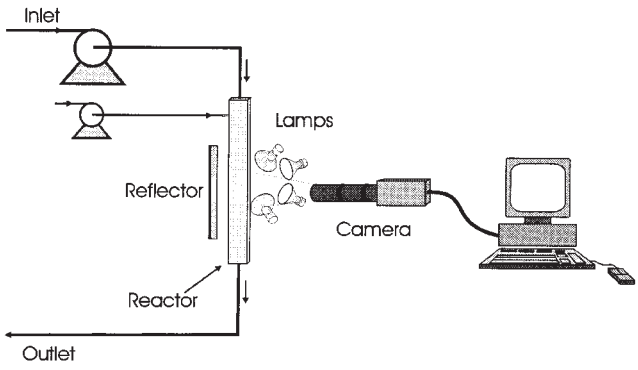

Figure 1. Experimental setup for the bubble and drop breakup measurements.

light source giving approximately one million lux had to be used to obtain enough focal depth. In all measurements the image resolution was 309,000 pixels/cm^2. This allowed the size of all fragments formed upon breakup to be measured. Optimization of the light source positions was required to obtain high quality images of the fluid particles passing the measurements area.

Besides the high-speed imaging system, the experimental facility, shown in Figure 1, consisted of a reactor and two pumps. The main pump allowed flow rates up to 250 liters per hour. In order to avoid turbulence modulation by the fluid particles, the experiments were performed at very low dispersed phase hold-up. The objective was to inject bubbles and drops one by one. By using injection nozzles of different diameters, gas bubbles and liquid drops with different sizes could be created. Three different systems were investigated, namely: air-water, dodecane-water, and octanol-water. Air-water and dodecane-water were chosen because of their similar interfacial tension. The observed difference will then mainly be attributed to their difference in density and viscosity. In contrast to dodecane-water, octanol has higher viscosity and much lower interfacial tension. This means that the Ohnesorge number will be higher and viscous effects could not be neglected for the octanol-water system. The physical properties of these three systems are given in Table 1.

Except for the octanol system, the Ohnesorge number, $Oh = \mu_d/(\rho_d d\sigma)^{1/2}$, which characterizes the viscous to interfacial forces, was kept low. When the Ohnesorge number is very small, $Oh < 0.01$, the internal viscous stress is negligible compared to the interfacial stress and can be neglected. Typical values of the Ohnesorge number in these measurements were $0.001 < Oh < 0.01$ (for the air-water and dodecane-water systems). Hence, the cohesive force is due to the interfacial stress.

The measurements were performed at the flow conditions shown in Table 2. As shown in this table, there is always at least one condition that is the same for the different systems.

The reactor, shown in Figure 1, has transparent walls with no curvature. This allowed observations of the fluid particles without optical distortion. One of the main advantages of using this reactor is that high turbulence levels can be achieved at low flow rates. Due to the construction of the reactor, production and dissipation of turbulent kinetic energy occurs throughout the entire reactor and turbulence is much more homogeneous than in a stirred tank reactor. This is due to the fact that the reactor is built up from identical small mixing elements.[4] Previous studies of PIV and CFD data showed that the turbulence is very homogenous within each mixing element in the reactor.[4,17] The Taylor scale Reynolds numbers shown in Table 2 indicate that there exists an inertial sub-range but the overlap between production scales and dissipation scales is large. A Taylor scale Reynolds number of 77 corresponds to a Reynolds number of 66,000 in a straight pipe with the same hydraulic diameter.

Table 1. Physical Properties of the Systems Used in this Work

Phases Dispersed/ Continuous	Interfacial Tension σ_i [N/m]	Density ρ_d [kg/m^3]	Viscosity μ_d [Pas]
Air-water	0.072	1	2e-5
Dodecane-water	0.053	750	1.5e-3
Octanol-water	0.0085	819	6.5e-3

Table 2. Experimental Conditions

System/Flow Rate [1/h]	100	150	200	250
Turbulent energy dissipation rate, ε [m^2/s^3]	1.13	3.69	8.54	16.4
Taylor scale Reynolds number	51	61	69	77
Air-water	—	X	X	X
Dodecane-water	X	X	X	—
Octanol-water	X	X	—	—

The high turbulence levels is revealed not only by the CFD simulations and PIV measurements but also from the observations that fluid particles smaller than 1 mm easily breakup. Since this reactor produces high turbulence levels at low flow rates, it is excellent for study of the breakup of fluid particles, that is, it is easy to take sharp images during the deformation and breakup processes. Furthermore, since single fluid particles are introduced into the reactor, the dispersed phase hold-up is extremely low and the turbulent conditions are similar as for a single phase flow, that is, the turbulence modulation is negligible. Low hold-up not only ensures negligible turbulence modulation but also allows a correct identification of all fragments formed upon multiple breakup.

The turbulent field contains a lot of structures, as can be seen in Figure 2. When a fluid particle is immersed in a turbulent field, it experiences disruptive turbulent stresses. These stresses come from the high energetic turbulent structures within the bulk that interact with and transfer energy to the fluid particles. As seen in the high-speed recordings, the deformation and breakup processes of fluid particles are very structured and smooth when high enough temporal resolution is used. Hence, breakup of fluid particles in turbulent flows is best viewed as interaction and energy transfer between high energetic structures within the bulk and fluid particles, not as random fluctuations that cause breakup. By analyzing the breakup process in detail, it is revealed that the breakup of bubbles and drops differs in many interesting ways.

Results and Discussion

The high spatial and temporal resolution allowed the breakup phenomenon to be studied in detail. Analysis of the experimental data include: measurement of the deformation degree, deformation velocity, breakup time, resulting fragment sizes, and number of fragments formed upon breakup. By performing the experiments in the same reactor, under identical conditions, a comparison between bubble and drop breakup is straightforward. In this section the differences between bubble and drop breakup are discussed. The analysis is based on about 200,000 pictures. Approximately 3000 observations of breakup were noted, and 300 of these breakups were followed in detail.

Deformation prior to breakup

To describe the interaction between turbulent structures and the motion and deformation of the fluid-fluid interfaces, it is good to separate the deformations into different scales. Since there is no given nomenclature for these scales, we will refer to

Figure 2. Structures in turbulent flows.

(a) Contours of iso-vorticity 800 [1/s] from LES simulations, (b) z-vorticity component and vector field obtained with PIV measurements. [Color figure can be viewed in the online issue, which is available at www.interscience.wiley.com.]

them as micro, meso, and macro scale deformations, although they all occur on the scale of the fluid particles, which at least from an engineering perspective is on the micro scale.

Micro-scale deformations—ripples

Experimental observations showed that, while bubbles have small scale high frequency deformations at the interface, such deformations are not present at the drop interfaces. These deformations look like small scale ripples on the interface and give no deformations of the entire fluid particle. The time scale of these small scale fluctuations at the gas-liquid interfaces are about one order of magnitude or less than the time scale for bubble breakup. Since the ripples occur on such small length scales and the time scale is much lower than the time scale of eddies on the size of the fluid particles, this implies that they are caused by eddies much smaller than the fluid particle itself. The small scale ripples do not cause large scale amplitudes; instead, the energy is dissipated rapidly. These interfacial ripples are less pronounced for small bubbles since the interfacial stress resisting the ripple formation scales as σ/d. The reason the ripples do not exist at drop interfaces is that the energy contained in the small eddies is not sufficient to accelerate the corresponding mass in a drop, which has three orders of magnitude higher inertia compared to air. Hence, the small scale fluctuations are restored quickly and do not contribute to the breakup of bubbles.

Meso-scale deformations—oscillations

Meso-scale deformations or oscillations were observed in the measurements. In contrast to the micro-scale deformations, these deformations result in deformations of the entire particle. The meso-scale oscillations seem not to amplify themselves; instead, they have a narrow range of amplitude. The typical deformation degree associated with the meso-scale oscillations is $l/d_0 \sim$ 1.1-1.3, whereas the macro deformation that results in breakup lies within the range $l/d_0 \sim$ 2-3. Thus, the meso scale deformations do not cause breakage.

Macro-scale deformations

It was observed that the interaction between turbulent eddies and fluid particles often results in large scale deformations. The time scale of the large scale deformations is typically on the order of the large energy containing eddies in the system, and the deformation typically occurs over scales that are 2- 3 times the initial diameters, that is, $l/d_0 \sim$ 2-3. Interestingly, the deformation is very structured in the sense that it occurs in a given direction. This implies that the fluid particle interacts with one eddy or a pair of eddies, not an array of eddies. The outcome from these large scale deformations is either a rapid relaxation to the spherical state or a subsequent breakup into N fragments. The number of fragments and the fragments sizes differ significantly between bubble and drop breakup.

Analysis of the deformation degree of fluid particles reveals how much energy has been transferred from the turbulent structures to the fluid particles before breakup occurs. From the measurements, it is seen that as an intermediate step in the breakup process, the deformed fluid particles are highly deformed. Physically this state can be seen as an activated complex in analogy to an activated complex in a chemical reaction. At this state the activated complex has an interfacial area that is larger than the sum of the daughter fragments. Thus, an energy transfer larger than the one corresponding to the energy of the resulting daughter fragments must be transferred from a turbulent eddy to reach this activation energy. Hence, defining a breakup criterion based on the interfacial energy increase for the resulting daughter fragments, as done in many breakup models found in the literature, leads to an underestimation of the energy that is required for breakup.

The degree of deformation can be represented by either the aspect ratio, α, which defines the ratio between the two characteristic deformation axes, $\alpha = l_1/l_2$, or by $z=l_1/d_0$. In this study the latter definition, the ratio between the long axis and the initial bubble diameter, is used. In the analysis the shape of the deformed complex is approximated by a cylinder with two spherical ends. Furthermore, in the analysis of the energy

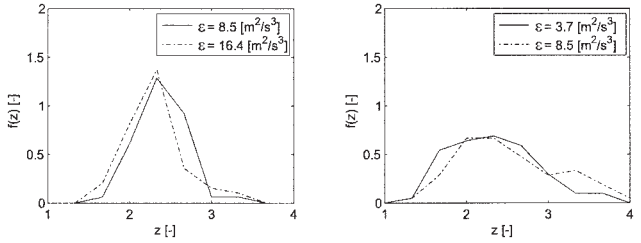

Figure 3. Distribution of deformation prior to breakup at different hydrodynamic conditions. (a) bubble deformation, and (b) drop deformation.

required to deform fluid particles, the inertia is neglected. Our calculations show that inertia can be significant for larger liquid drops but not for gas bubbles due to the difference in density. In this study, only deformation and breakup of small fluid particles is studied. Hence, the effect of inertia during deformation is negligible.

Measurements of the bubble and drop deformations prior to breakup were made at different flow rates. Figure 3 shows that the deformations at the two flow rates are similar. Thus, the deformations are constant regardless of the dissipation rate. This is thought to be a result of the fact that when the fluid particles are at their equilibrium sizes, the cohesive and disruptive stresses are close to equal regardless of flow rate.

The degree of deformation for bubbles and drops in the same background turbulence, that is, $\varepsilon = 8.5$ [m^2/s^3], is shown in Figure 4. The average deformation is approximately equal, although the variance is larger for drops than for bubbles. On average the deformation degree equals 2.5. This corresponds to an interfacial energy increase of 34%. The vast majority of all breakup models proposed in the literature assume that only binary breakup occurs and use some criterion based on the energy increase to predict if breakup occurs and the probability for creating daughter fragments of given sizes. The maximum increase in interfacial energy, assuming binary breakup, equals 26%. Hence, defining a breakup criterion on the resulting interfacial energy increase is not good, since it consequently underestimates the energy required for breakup. More importantly, it does not describe the physics of the breakup process,

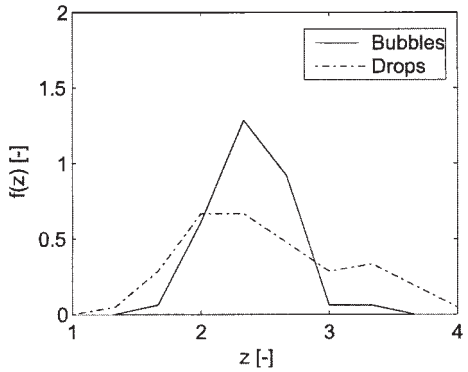

Figure 4. Comparison of bubble and drop deformation in the same background turbulence, $\varepsilon = 8.5$ [m^2/s^3].

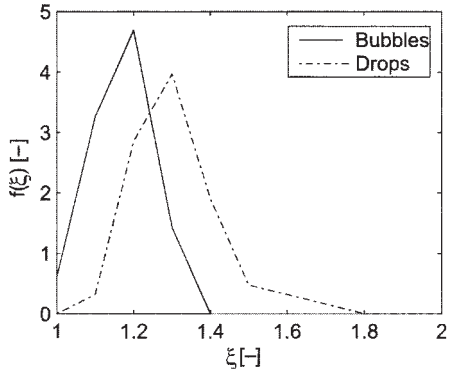

Figure 5. PDF of the dimensionless energy increase for bubble and drop after breakup, $\varepsilon = 8.5$ [m^2/s^3].

that is, the activation energy that must be reached before breakup occurs.

An analysis of the energy increase associated with the resulting daughter fragments, that is, after breakup, is straightforward, in that it requires neither an assumption of the inertia during breakup nor an assumption of the shape of the deformed complex. The interfacial energy increase after breakup is shown in Figure 5. The measurements were performed at the same hydrodynamic conditions, $\varepsilon = 8.5$ [m^2/s^3]. For binary breakup the breakup volume fraction, f_{bv}, uniquely describes the thermodynamic increase in interfacial energy. Assuming that breakup is binary, the dimensionless energy increase due to a single breakup is given by:

$$\xi = (d_1^2 + d_2^2)/d_0^2 = f_{bv}^{2/3} + (1 - f_{bv})^{2/3} \tag{9}$$

Equation 9 goes through a maximum at $f_{bv} = 0.5$ where $\xi = 126$. Thus, equal sized breakup corresponds to the highest energy uptake and the energy increase for binary breakup is bounded by $1 < \xi \leq 1.26$.

Analysis of the experimental data reveals that the energy increase is much lower for bubbles than for drops. Figure 5 shows that the average energy increase is approximately 75% larger for drops than for bubbles. In addition, the energy increase for drop breakup often exceeds levels that can be explained with the binary breakup mechanism. Obviously, the assumption of binary breakup does not hold for drop breakup.

Most interesting, however, is that although both bubble and drop breakups are subject to large deformations and approximately equal amounts of energies are transferred to the deformed complexes, significantly less energy remains after breakup for bubbles than for drops, as shown in Figures 4 and 5. This difference is due to an internal flow mechanism. The figures show that more energy is transferred to the fluid interface in the initial stage of breakup than what remains after breakup. Hence, more energy is required to overcome the initial stage of deformation than for creating two fragments of unequal size. The change in interfacial energy during the bubble breakup process is schematically shown in Figure 6, where an activation energy barrier is included.

An estimation of the time scale for breakup and efficiency of energy transfer can be found by comparing the time for bubble

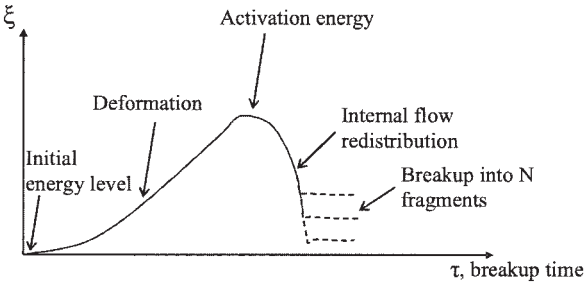

Figure 6. Interfacial energy during the breakup process.

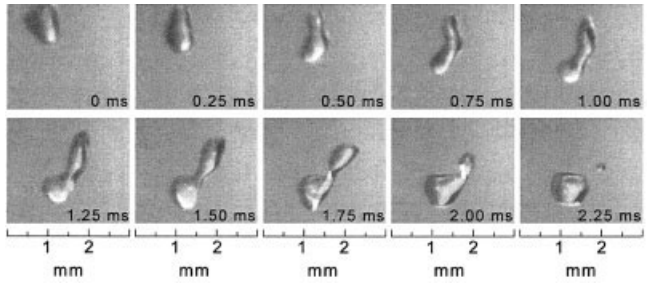

Figure 7. Breakage of a gas bubble into two fragments of different size; water-air, ε = 16 m²/s³, τ = k/ε = 6 [ms].

and drop breakup with the turbulent time scales. Table 3 reveals that the average time for bubble and drop breakup is in the range of 1/2 to 2/3 of the turbulent time scale k/ε. These long time scales indicate that only large turbulent eddies are effective in bubble and drop breakup.

Internal flow redistribution

The mechanism responsible for the difference between bubble and drop breakup is mainly the internal flow mechanism. In Figure 7, where the breakup of a 1 mm gas bubble recorded at 4000 Hz is shown, the initial stage of the breakup process is characterized by a fairly symmetrical deformation. At this stage the bubble is subject to a disruptive stress given by Eq. 1.

After approximately 1 ms, the rate of deformation decreases because the turbulent structure has lost a large part of its energy. When the turbulent eddy starts to lose its energy, the pressure within the bubble will be more and more determined by the surface tension and local curvature. Although the deformed bubble is rather symmetrical, small size differences between the two ends typically exist. This is a result of how the turbulent eddy and the bubble interact and the background turbulence in the vicinity of the bubble. The asymmetry causes an internal pressure difference between the two ends of the deformed bubble. This pressure difference arises because the curvature is not the same at the two ends of the deformed complex. When the turbulent eddy lost all its energy, the internal pressure difference equals

$$\Delta p_{\text{int}} = \frac{2\sigma}{r_1} - \frac{2\sigma}{r_2} \tag{10}$$

where r_1 and r_2 are the radii of the two ends. Initially the effect of the internal pressure difference is low. As a result of the pressure difference in the deformed bubble, the gas starts to flow to the low pressure side of the bubble and the deformed bubble becomes even less symmetrical. At this stage the internal flow is accelerated as the sizes of the two ends become more unequal. The effect of this acceleration can be observed in Figure 7. The internal redistribution of gas accelerates rapidly and the time scale for redistribution is about 1 ms. When breakup eventually occurs, two fragments of unequal sizes are formed. Depending on how much mass has been redistributed, the ratio of the fragments volumes can become very large. In this case the breakup volume fraction is $f_{bv} = 0.98$. From static stress analysis, it can be found that an instability appears when the neck become smaller than 1/2 to 1/3 of the bubble end diameter. At this point the pressure in the neck due to interfacial tension will be higher than at the ends and gas will flow from the neck and the fluid particle breaks.

The internal flow mechanism is frequently occurring. This is easily seen in the bubble daughter size distribution. The size distribution clearly shows that unequal sized daughter fragments often are formed. The daughter size PDF has highest probability for unequal-sized breakup, which is attributed to this mechanism. Since two fragments of different sizes often are formed, the increase in interfacial energy after breakup becomes low. In contrast, this mechanism does not occur for drop breakup. This is due to the fact that the density of liquids is three orders of magnitude higher than for gases. Consequently, the pressure difference is not sufficient to cause an internal mass redistribution. Thus, drops often breakup into fragments of equal size, which implies a larger increase in the interfacial energy. This mechanism explains differences in interfacial energy increase between bubbles and drops shown in Figure 5.

While, most models proposed in the literature predict highest probability for unequal-sized fragmentations, this occurs only for bubbles not for drops. In contrast to what is assumed, this is not due to that a small fragment is ripped off; rather, it is an effect of the internal flow redistribution. Hence, assumption of small eddies that rip off small fragments is wrong. The energy contained in small eddies is not sufficient to cause the increase in interfacial energy for the deformed complex; it may just be

Table 3. Time for Bubble and Drop Breakup in Comparison to the Turbulent Time Scale

	100		150		200		250	
Flow rate l/h	$\langle\tau\rangle$ ms	σ^2 (ms)^2	$\langle\tau\rangle$ ms	σ^2 (ms)^2	$\langle\tau\rangle$ ms	σ^2 (ms)^2	$\langle\tau\rangle$ ms	σ^2 (ms)^2
Water-air					3.8	1.2	3.4	0.9
Water-dodecane			7.6	2.7	4.2	1.1		
Water-octanol	10.9	4.9	5.6	1.2				
k/ε	15		10		7.5		6.0	

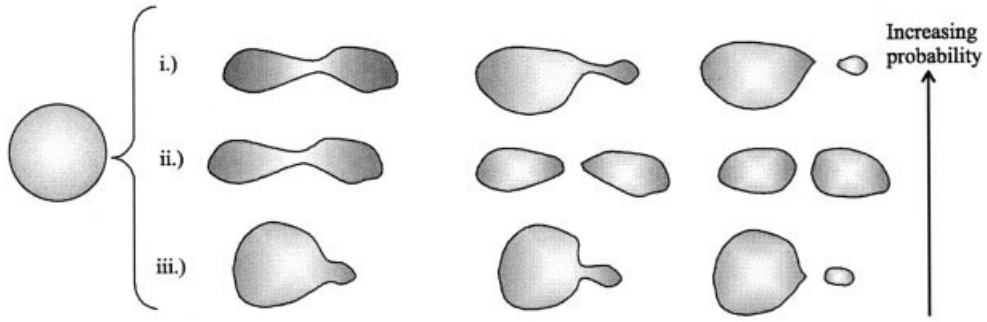

Figure 8. Gas bubble breakup.

(i) Deformation with subsequent redistribution and breakup. (ii) Deformation and breakup without internal redistribution. (iii) Direct breakup into unequal-sized fragments.

large enough to match the resulting increase after breakup. It is not likely that small eddies can cause large deformations typically 2.5 times the bubble diameter, $l_l/d_0 \sim$ 2-3. The probability for gas bubble breakup is illustrated in Figure 8.

These experimental observations, along with the analysis of the disruptive, cohesive stresses, and energies involved, imply that turbulent eddies close in size to the bubbles are responsible for breakup. Hence, it not reasonable to account only for eddies smaller than or equal to the bubble size in breakup rate models. It is well known that the theoretical models proposed in the literature are sensitive to the choice of the upper eddy size causing breakup. For a 1 mm gas bubble the overall breakup rate may be changed 1-2 orders of magnitude when accounting for eddies twice as large as the bubble rather than just equal to the bubble.[1] It is, therefore, important to account not only for the right breakup mechanisms of bubbles and drops but also to account for the correct bandwidth of turbulent eddies that cause breakup. In a recent article the authors proposed a new model for the overall breakup rate for bubbles and drops.[18] In this article it is described how the breakup mechanism and bandwidth can be modeled more accurately.

Daughter size distributions

Due to the different breakup mechanisms for bubble and drop breakup, the resulting daughter size distributions differ significantly. The analysis is actually difficult to make since drop breakup often results in multiple fragments. In contrast, bubbles are subject to binary breakup. In this analysis we define the breakup volume fraction as

$$f_{bv} = \frac{\nu_1}{\sum_{i=1}^{N} \nu_i} \tag{11}$$

where ν_1 is the volume of the largest fragment and $\sum_{i=1}^{N} \nu$ is the sum of all fragments. Thus, the daughter size distribution can be plotted as a one-dimensional function of f_{bv}. The statistics of the daughter size distributions are shown in Figure 9. Bubble breakup often results in unequal size fragments while drop breakup often results in equal sized fragments. The probability of creating unequal sized drop fragments is very low. No model proposed so far can predict this difference. By accounting for the internal flow mechanism, it would be possible to make this development. Further refinement of the breakup rate model also requires insight in the difference between binary and multiple fragmentations for bubbles and drops. Partly due to the lack of data on binary and multiple fragmentations and partly to simplify the mathematical treatment of the breakup rate models, binary fragmentation is often assumed in the literature.

Binary and multiple breakup

The vast majority of all models proposed for fluid particle breakup are based on assumptions that only binary breakup occurs. It is concluded that, for the experimental conditions in this study, most bubble breakup results in binary breakup. Analysis of the number of fragments formed upon bubble breakup showed that the probability for binary fragmentation is equal to or larger than 95%. In contrast, multiple fragmentations often occur when drops break up; in fact, multiple breakage has higher probability than binary breakup for liquid drops. In Figure 10, three fragments are formed upon breakup of a liquid drop. Although the smallest fragment is of equal size as the fragment in the bubble breakup, the mother particle size is significantly reduced, which is not the case for bubble breakup. Hence, in contrast to bubble breakup, small fragments may be formed upon drop breakup, although not affecting significantly the rate at which the mother particles size is reduced.

Analysis of the experimental data shows that the probability for binary drop breakup is less than 40%. The number frequency functions measured at two flow conditions are shown in Figure 11. Although multiple breakup is the most frequent

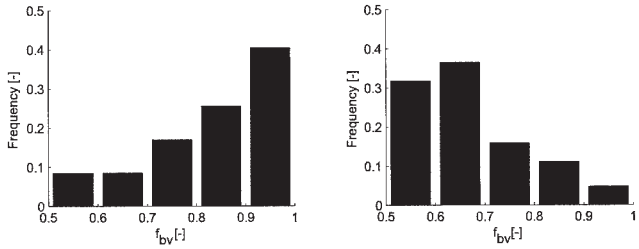

Figure 9. Statistics of bubble and drop breakup for the same hydrodynamic conditions, ε = 8.5 [m^2/s^3].

(a) Gas bubbles, and (b) liquid drops; volume fraction of the largest fragment.

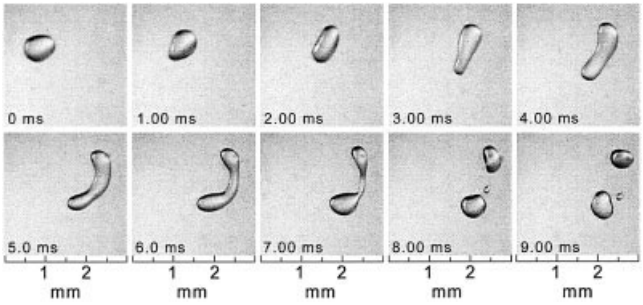

Figure 10. Breakage of a liquid drop into three fragments of different sizes; water-dodecane, ε = 8.5 [m^2/s^3], $\tau = k/\varepsilon = 8$ [ms].

outcome, binary breakup may still be a reasonable assumption, if the volume and even more importantly the interfacial area of the residual fragments are negligible. The important question is then how much the additional fragments contribute to the increase in interfacial area. This may be quantified by analyzing the cumulative contribution of each fragment to the increase in interfacial area.

In Figure 12, the cumulative contributions of both the volume fraction and interfacial area are shown as a function of the fragment number. In this analysis the fragment sizes are sorted in decreasing sizes. As seen in Figure 12, the two main fragments formed upon breakup contribute on average to 92% of the increase in interfacial area and 96% of the volume of the initial drop volume. Thus, neglecting the contribution of the small fragments gives on average an underestimation of 8% of the interfacial area. Since this underestimation is per breakup event, the overall underestimation may be very large. Since the coalescence rate is proportional to the fluid particle number density squared, a severe underestimation may be introduced for the coalescence rate.

To conclude, the initial deformations of bubbles and drops are similar although the resulting fragment sizes and number of fragments differ. The characteristics of bubble and drop breakup are given in Table 4.

Breakup of viscous drops

For small drops and drops with high viscosity, the internal viscous effects are not negligible. Under such conditions the deformed drop can become highly deformed before it eventually breaks up into a number of fragments. As shown in Figure 13 where the breakup of an octanol drop is shown, the deformed complex seems to wind around a rotating fluid element. It is reasonable that viscous shear contributes to the breakup process. This is not so with bubbles, for which only the normal stresses contribute to breakup.

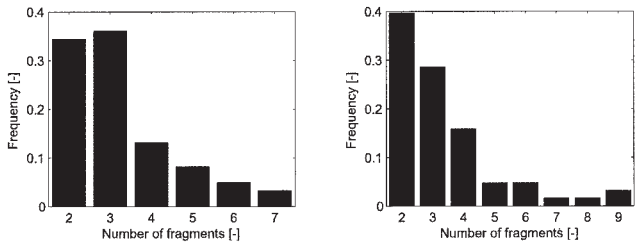

Figure 11. Number probability function for drop breakup, dodecane-water system.

(a) ε = 3.7 [m^2/s^3], and (b) ε = 8.5 [m^2/s^3].

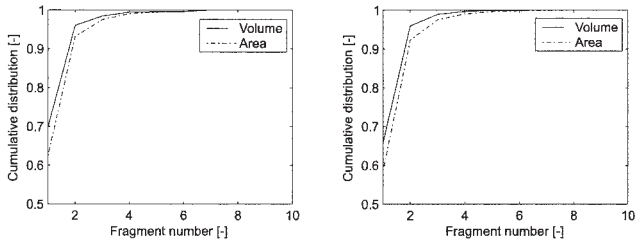

Figure 12. Cumulative contribution to volume and interfacial area as function of the number of fragments, dodecane-water system.

(a) ε = 3.7 [m^2/s^3], and (b) ε = 8.5 [m^2/s^3].

Often the deformation of small viscous drops results in formation of thin liquid threads, which can be identified in the last three images in Figure 13. The threads formed between the two main ends of the deformed complex can become 20 times larger than the initial drop diameter. When these threads break, many very small fragments are formed. Further analysis of fluid particle breakup and in particular breakup of viscous drops requires knowledge of the energy transfer across interfaces in turbulent flow.

Energy transfer at fluid-fluid interfaces

It is an interesting question whether there is a significant difference in momentum transfer across gas-liquid and liquid-liquid interfaces that affects the breakup of bubbles and drops. Traditionally only the normal stresses, that is, the dynamic pressure fluctuation of the turbulent eddies, are accounted for in the literature. From studies of the drag coefficient in systems with different interface rheology, it is known that the drag differs from gas-liquid, liquid-liquid, and solid-liquid systems. The gas-liquid interface can be approximated by a shear-free boundary condition when no interfacial tension gradient exists at the interface. This is due to the low viscosity ratio between the phases. This means that the contribution of the viscous drag to the total drag for a gas bubble in a liquid is negligible. In contrast, the momentum transfer across liquid-liquid interfaces is more efficient due to the contribution viscous drag. Unfortunately, the models that exist for turbulent conditions are very uncertain. If there exists a significant difference in momentum transport across gas-liquid and liquid-liquid interfaces, there will consequently be a difference in the energy transfer that could affect the breakup of fluid particles. One way to study this would be to simultaneously measure the flow around a

Table 4. Important Characteristics of Bubble and Drop Breakup

Characteristic Feature	Bubbles	Drops
Deformation degree	Large scale	Large scale
Internal flow mechanism	Yes	No
Daughter size PDF	Unequal-sized	Equal-sized
Fragmentation	Binary	Multiple

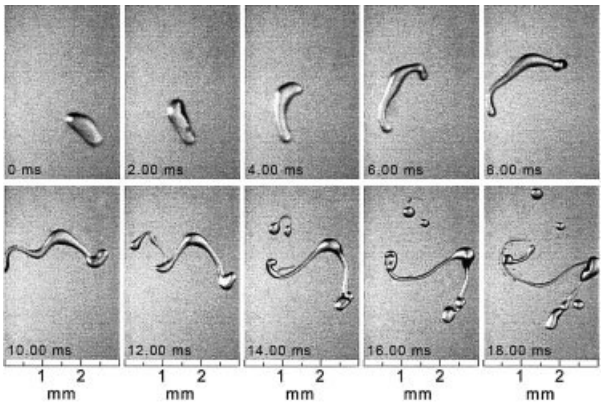

Figure 13. Breakage of a viscous drop into several fragments of different sizes; water-octanol, ε = 3.7 [m^2/s^3], $\tau = k/\varepsilon$ = 10 [ms].

single fluid particle during deformation and breakup. When such techniques are developed, this would be helpful in determining whether such differences must be included to describe the breakup process correctly.

Conclusions

In this work the dynamics of the deformation and breakup processes of fluid particles in turbulent flows were studied by using a high-speed video imaging technique. The experimental studies of both bubbles and drops were made in the same reactor under identical operating conditions, which made a comparison between bubble and drop breakup dynamics straightforward. It is concluded from this study that there are several differences in the breakup mechanisms of bubbles and drops.

Although the initial stage of the breakup process is equal for bubbles and drops, the outcome differs in two important ways. The fist difference concerns the resulting daughter size distribution. The measurements showed that while bubbles often result in fragments of unequal size, drops form equal-sized fragments. This was explained by an internal flow redistribution mechanism, active only for bubbles. This mechanism caused an internal redistribution and thereby generated fragments of different sizes. In contrast, drops broke up without such a mechanism, thereby generating fragments of equal size.

The second important difference between bubbles and drops concerns the number of fragments formed upon breakup. It was also found that bubble breakup mainly results in two fragments. In contrast, drops rarely formed only two fragments upon breakup. Instead, drops stretched until the neck became thin and broke up. Often there were several smaller fragments formed between the two larger ends.

One important conclusion is that the breakup process itself is best described by its dynamics and is not well described as a state function where only the initial condition and the outcome are accounted for. It was found that the required energy transfer often exceeded what can be explained by only accounting for the resulting energy increase in the fragments. This implies the requirements on the eddy energies are underestimated in most models proposed in the literature.

The major conclusions from this work can be summarized as:

- The initial deformations of bubbles and drops are similar, although the resulting fragment sizes and numbers of fragments differ.
- During the breakup process an activated complex is formed that contains more energy than the resulting fragments.
- The breakup of gas bubbles and liquid drops results in a wide range of fragments sizes, with size distribution PDF's that are completely different.
- During the bubble breakup process, an internal flow redistribution occurs, as a result of internal pressure differences experienced by the bubble.
- Due to the internal flow redistribution, unequal size fragments are often formed. Hence, the unequal sized breakup of gas bubbles is not a result of splitting of a small fragment; instead, the small fragments are formed due to the internal flow redistribution.
- In contrast, equal sized breakup is the most probable outcome for drop breakup.
- While binary breakup is most likely for gas bubbles, multiple fragmentation is most likely for liquid drops.
- Breakup of viscous drops often results in highly deformed complexes that wind themselves around the turbulent eddies. Deformations up to 20 times the initial drop diameter were observed in this work.

Notation

d = drop diameter, m
e = eddy energy, kg m^2 s^{-2}
$\bar{e}$ = mean eddy energy, kg m^2 s^{-2}
p = pressure, Pa
P = probability function, -
$\bar{u}_\lambda$= mean velocity fluctuations, m s^{-1}

Greek letters

ε = turbulent energy dissipation rate per unit mass, m^2 s^{-3}
λ = eddy size, m
μ = dynamic viscosity, kg m^{-1} s^{-1}
ν = kinematic viscosity, m^2 s^{-1}
ρ = density, kg m^{-3}
σ = interfacial tension, kg s^{-2}
τ = stress, kg m^{-1} s^{-2}

Superscripts and subscripts

c = continuous phase
d = dispersed phase
int = internal

Literature Cited

1. Lasheras JC, Eastwood C, Martinez-Bazan C, Montanes JL. A review of statistical models for the break-up of an immiscible fluid immersed into a fully developed turbulent flow. *Int J Multiphase Flow.* 2002;28: 247-278.
2. Kolmogorov AN. On the breakage of drops in a turbulent flow. *Dokl Akad Nauk SSSR.* 1949;66:825-828.
3. Hinze JO. Fundamentals of the hydrodynamic mechanism of splitting in dispersion processes. *AIChE J.* 1955;1:289-295.
4. Andersson R, Andersson B, Chopard F, Noren T. Development of a multi-scale simulation method for design of novel multiphase reactors. *Chem Eng Sci.* 2004;59:4911-4917.
5. Venneker BCH, Derksen JJ, Van den Akker HEA. Population balance

modeling of aerated stirred vessels based on CFD. *AIChE J.* 2002;48: 673-685.
6. Nienow AW. Break-up, coalescence and catastrophic phase inversion in turbulent contactors. *Advances Colloid Interface Sci.* 2004;108–109:95-103.
7. Luo H, Svendsen HF. Theoretical model for drop and bubble breakup in turbulent dispersions. *AIChE J.* 1996;42:1225-1233.
8. Baldyga J, Bourne JR, Pacek AW, Amanullah A, Nienow AW. Effects of agitation and scale-up on drop size in turbulent dispersions: allowance for intermittency. *Chem Eng Sci.* 2001;56:3377-3385.
9. Risso F, Fabre J. Oscillations and breakup of a bubble immersed in a turbulent field. *J Fluid Mechanics.* 1998;372:323-355.
10. Sleicher JCA. Maximum stable drop size in turbulent flow. *AIChE J.* 1962;8:471-477.
11. Collins SB, Knudsen JG. Drop-size distributions produced by turbulent pipe flow of immiscible liquids. *AIChE J.* 1970;16:1072-1080.
12. Konno M, Aoki M, Saito S. Scale effect on breakup process in liquid-liquid agitated tanks. *J Chem Eng Japan.* 1983;16:312-319.
13. Walter JF, Blanch HW. Bubble break-up in gas-liquid bioreactors: break-up in turbulent flows. *Chem Eng J.* 1986;32:B7-B17.
14. Hesketh RP, Etchells AW, Russell TWF. Experimental observations of bubble breakage in turbulent flow. *Ind Eng Chem Res.* 1991;30:835-841.
15. Martinez-Bazan C, Montanes JL, Lasheras JC. On the breakup of an air bubble injected into fully developed turbulent flow. Part 1. Breakup frequency. *J Fluid Mechanics.* 1999;401:157-182.
16. Eastwood CD, Armi L, Lasheras JC. The breakup of immiscible fluids in turbulent flows. *J Fluid Mechanics.* 2004;502:309-333.
17. Bouaifi M, Mortensen M, Andersson R, Orciuch W, Andersson B. Experimental and numerical investigations of jet mixing in a multifunctional channel reactor: passive and reactive systems. *Chem Eng Res Design.* 2004;82:274-283.
18. Andersson R, Andersson B. Modeling the breakup of fluid particles in turbulent flows. AIChE J. 2006; in press.

Manuscript received Oct. 6, 2005, and revision received Feb. 11, 2006.